2014 IEEE International Conference on Robotics & Automation (ICRA)
Hong Kong Convention and Exhibition Center
May 31 - June 7, 2014. Hong Kong, China

Magnetic-Based Closed-Loop Control of Paramagnetic Microparticles using Ultrasound Feedback

Islam S. M. Khalil[1], Pedro Ferreira[2], Ricardo Eleutério[2], Chris L. de Korte[3] and Sarthak Misra[4]

***Abstract*— Controlling the motion of microrobots based on feedback provided using an imaging modality is essential to make them clinically viable. In this study, we demonstrate the wireless magnetic-based motion control of paramagnetic microparticles using ultrasound feedback. This control is accomplished by pulling the microparticles using the magnetic field gradients towards the reference position through feedback provided by an ultrasound system. First, position of the microparticles is determined using the ultrasound images. Second, calibration of the ultrasound-based tracking of microparticles is achieved and verified using a calibrated microscopic system. Third, the feedback provided by the ultrasound system is used in the implementation of a proportional-derivative magnetic-based control system. This control system allows us to achieve point-to-point control of microparticles with an average position tracking error of 48±59 μm, whereas a control system based on a microscopic system achieves an average position tracking error of 21±26 μm. The positioning accuracy accomplished using our ultrasound magnetic-based control system demonstrates the ability to control microrobotic systems in situations where visual feedback cannot be provided via microscopic systems.**

I. INTRODUCTION

There exists at least three main challenges that stand between the utilization of microrobotic systems in magnetic-based targeted drug delivery. First, realization of wireless magnetic-based control using feedback provided by a clinical imaging modality [1], [2]. Second, the ability to steer microrobots through relatively large distances by pulling with the magnetic field gradients [3], [4], or moving using self-propulsion [5]. Third, the ability of magnetic systems and their controllers to compensate for the time-varying flow rates [6], [7], surface effects, channel wall effects [8], and time-varying viscosity in a medium.

Evertsson *et al*. used a high-frequency ultrasound scanner to evaluate the motion of superparamagnetic iron oxide nanoparticles, by developing an algorithm based on quadrature detection and phase gating at the frequency of interest [9], [10]. This algorithm could allow for providing feedback and controlling the motion of nanoparticles using ultrasound feedback. Martel *et al.* presented a medical nanorobotic interventional platform that uses a magnetic resonance imaging for feedback of the position and control of magnetic drug carriers, nanorobots, and magnetotactic bacteria *in vivo* [1]. However, a major disadvantage in using a magnetic resonance imaging system for tracking and actuation is the possibility of inducing time-delay due to communications and interactions between the various modules of the interventional platform. This time-delay could cause instability in the closed-loop control system and possibly limit the realization of the control system in real-time.

In this work, we demonstrate the closed-loop motion control of paramagnetic microparticles using an ultrasound system. Ultrasound has no unfavorable effects on health, adequate resolution and high frame rates that allow for the realization of real-time control, and low cost, as opposed to magnetic resonance imaging and computed tomography [3]. We integrate an ultrasound system to our magnetic-based

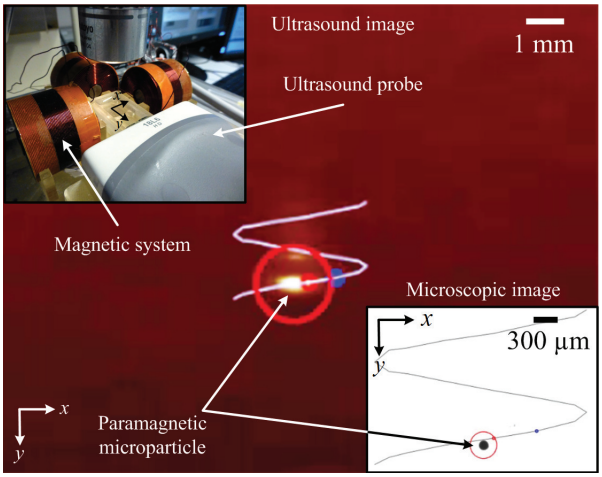

Fig. 1. Magnetic system with an ultrasound probe, i.e., 18L6 HD (upper-left inset), for the wireless motion control of paramagnetic microparticles (PLAParticles-M-redF-plain from Micromod Partikeltechnologie GmbH, Rostock-Warnemuende, Germany). Position of a single microparticle is determined using an ultrasound system (Siemens ACUSON S2000, Siemens Healthcare, Mountain View, USA). This position is also determined using a microscopic system to evaluate the accuracy of the ultrasound-based motion control of microparticles. The bottom-right inset shows a controlled microparticle following a sinusoidal trajectory under the influence of the controlled magnetic field gradients and using ultrasound feedback. The red circle indicates the microparticle and is assigned by our feature tracking algorithm [11], whereas the small red and blue circles are way points along the reference trajectory [12].

This work was supported by funds from MIRA–Institute for Biomedical Technology and Technical Medicine, University of Twente, The Netherlands.
[1]Islam S. M. Khalil is affiliated with the German University in Cairo, New Cairo City, Egypt islam.shoukry@guc.edu.eg
[2]Pedro Ferreira and Ricardo Eleutério are affiliated with the New University of Lisbon, Monte de Caparica, Portugal pr.ferreira,r.eleuterio@campus.fct.unl.pt
[3]Chris L. de Korte is affiliated with MUSIC–Medical Ultrasound Imaging Center, Radboud University Nijmegen Medical Centre, The Netherlands chris.dekorte@radboudumc.nl
[4]Sarthak Misra is affiliated with MIRA–Institute for Biomedical Technology and Technical Medicine, University of Twente, The Netherlands s.misra@utwente.nl

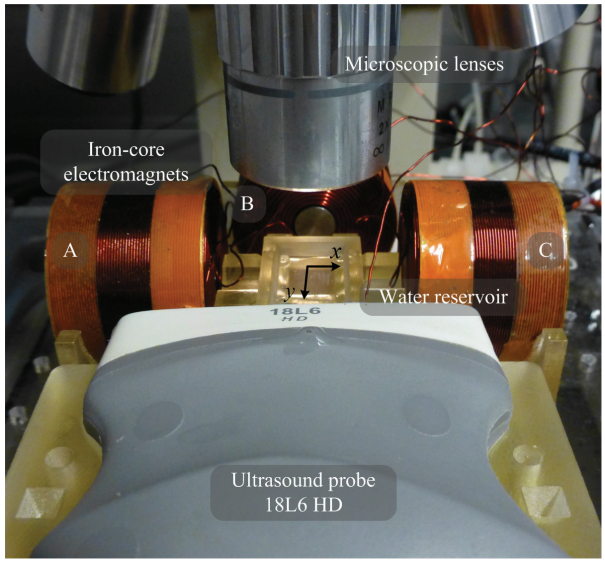

Fig. 2. An array of iron-core electromagnetic coils surrounding a water reservoir. This reservoir contains paramagnetic microparticles (PLAParticles-M-redF-plain from Micromod Partikeltechnologie GmbH, Rostock-Warnemuende, Germany). Position of the microparticles is determined using an ultrasound probe (18L6 HD, Siemens Healthcare, Mountain View, USA) and a microscopic system. Motion control is implemented based on the feedback provided using the ultrasound probe and compared to that based on the microscopic system. The microscopic system is also used to calibrate the ultrasound system and evaluate the accuracy of the ultrasound feedback.

manipulation system to provide feedback (Fig. 1). This feedback allows us to implement closed-loop motion control of microparticles using ultrasound feedback. Further, we compare the accuracy of the ultrasound-based closed-loop control to a microscopic-based control system.

The remainder of this paper is organized as follows: Section II provides a model of our magnetic system and a finite element (FE) simulation of the magnetic field gradients within the workspace of our system. In addition, we calibrate our ultrasound system and verify this procedure using a calibrated microscopic system. Closed-loop motion control of microparticles using ultrasound feedback is provided in Section III, along with a discussion pertaining to the control of microparticles using ultrasound feedback. Finally, Section IV concludes and provides directions for future work.

II. MODELING AND CALIBRATION OF THE ULTRASOUND-BASED MAGNETIC SYSTEM

Wireless control of paramagnetic microparticles is accomplished using an array of iron-core electromagnets and an ultrasound system. In this section, we model the magnetic force on the microparticles using an FE model, and calibrate the ultrasound system.

A. Magnetic System

Motion of the microparticles (PLAParticles-M-redF-plain from Micromod Partikeltechnologie GmbH, Rostock-Warnemuende, Germany, with an average diameter of 100 μm) under the influence of the magnetic field gradients is in the order of micrometers. Detecting this motion using an ultrasound probe (18L6 HD, Siemens Healthcare, Mountain View, USA) shows that it can be easily confused with undesirable motion artifacts. We observe that these motion artifacts are reduced by decreasing the distance between the ultrasound probe and the microparticles. Therefore, the probe of our ultrasound system (Siemens ACUSON S2000, Siemens Healthcare, Mountain View, USA) is placed at 25 mm from the center of the workspace of our magnetic system. The imaging depth is 35 mm. The magnetic system consists of 3 iron-core electromagnets. The array of electromagnets generates a maximum magnetic field of 15 mT, and magnetic field gradient in excess of 60 mT/m. The workspace of the electromagnetic arrangement is 2.4×1.8 mm^2 within the center of the reservoir shown in Fig. 2.

Investigating the relation between the magnetic fields, field gradient and the applied current at each of the electromagnet is essential for the implementation of a magnetic-based closed-loop control system. In a prior study using a configuration of 4 orthogonal electromagnets, we showed that the relation between magnetic fields and the current input is linear for iron-core electromagnets [13]. We further showed that the magnetic field gradients are almost uniform within the workspace of the 4 electromagnets. Linearity and uniformity of the magnetic field- and field gradient-current, respectively, allows us to simplify the implementation of the closed-loop control system.

First, magnetic field-current linearity of the iron-core electromagnets is verified. Increasing and decreasing currents are applied to the electromagnet, and then magnetic fields are measured at a representative point within the workspace of our magnetic system using a calibrated three-axis Hall magnetometer (Sentron AG, Digital Teslameter 3MS1-A2D3-2-2T, Switzerland) [13]. This linearity allows us to calculate the magnetic fields generated using the 3 electromagnets by superposition. Second, we calculate the magnetic field gradients within the workspace of our magnetic system. A validated FE model of our magnetic system is developed using Comsol Multiphysics® (COMSOL, Inc., Burlington, U.S.A). Current inputs of 0.1 A, 0.2 A, and 0.3 A are applied to electromagnets A, B, and C, respectively (Fig. 2). These currents are devised based on the current limit on our electromagnets (i.e., 1 A). The calculated magnetic field gradients are shown in Fig. 3. We observe that the magnetic field gradients are almost uniform within our workspace. We further observe that the configuration of our electromagnetic coil provides sufficient pulling magnetic forces in all directions within the workspace of our magnetic system. This indicates that our microparticle is controllable within the workspace. These observations allow us to implement a closed-loop control system without calculating the magnetic field gradients at each point of the workspace based on a magnetic force-current map.

The magnetic force ($\mathbf{F}(\mathbf{P}) \in \mathbb{R}^{2\times1}$) on a microparticle at point ($\mathbf{P} \in \mathbb{R}^{2\times1}$) is given by [14], [15], [16]

$$\mathbf{F}(\mathbf{P}) = \nabla(\mathbf{m} \cdot \mathbf{B}(\mathbf{P})), \tag{1}$$

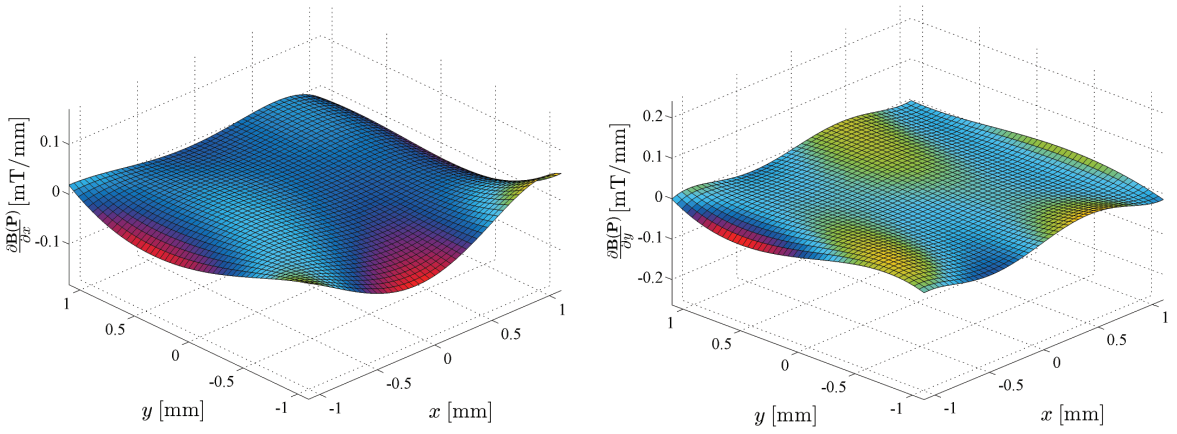

(a) Magnetic field gradient along x-axis

(b) Magnetic field gradient along y-axis

Fig. 3. Magnetic field gradients within the workspace of our magnetic system for current inputs of 0.1 A, 0.2 A, and 0.3 A at electromagnets A, B, and C, respectively (Fig. 2). The magnetic field gradients are almost uniform, and do not have to be calculated at each point of the workspace during the implementation of the ultrasound-based or microscopic-based closed-loop control of the microparticles. This simulation result shows that the modified configuration of the magnetic system allows microparticles to be pulled in all directions within the workspace of the magnetic system. This modification is done to incorporate the ultrasound probe and provide feedback to the closed-loop control system.

where $\mathbf{m} \in \mathbb{R}^{2\times 1}$ and $\mathbf{B}(\mathbf{P}) \in \mathbb{R}^{2\times 1}$ are the magnetic dipole moment of the microparticle and the induced magnetic field, respectively. The ith component of the magnetic force ($F_i(\mathbf{P})$) is given by the following magnetic force-current map [13]:

$$F_i(\mathbf{P}) = \beta \mathbf{I}^{\mathrm{T}} \left(\frac{\partial (\widetilde{\mathbf{B}}^{\mathrm{T}}(\mathbf{P}) \widetilde{\mathbf{B}}(\mathbf{P}))}{\partial i} \right) \mathbf{I} \quad \text{for} \quad i = x, y. \tag{2}$$

In (2), $\mathbf{I} \in \mathbb{R}^{3\times 1}$ and $\widetilde{\mathbf{B}}(\mathbf{P}) \in \mathbb{R}^{3\times 3}$ are the input current vector and a matrix that maps current onto magnetic fields, respectively. This map is calculated by the superposition of the contribution of each of the electromagnets based on the linearity of the magnetic field and current. Further, β is a magnetic constant and is given by

$$\beta \triangleq \frac{4}{3} \frac{1}{\mu} \pi r_{\mathrm{p}}^3 \chi_{\mathrm{m}}, \tag{3}$$

where r_{p} is the radius of a microparticle. Finally, χ_{m} and μ are the magnetic susceptibility constant and the magnetic permeability constant, respectively [14]. The magnetic force-current map is used in the implementation of a closed-loop control system of the microparticles based on feedback obtained using an ultrasound system. This ultrasound system is calibrated using a microscopic system.

B. Calibration of Ultrasound System

An ultrasound system cannot be calibrated directly from its ultrasound images using an object with known dimensions because of the undesirable artifacts that often appear in the ultrasound images. Therefore, we investigate an indirect method to calibrate our ultrasound system.

The experimental setup provides position feedback using an ultrasound system and a microscopic system. Although our closed-loop control is based on feedback provided using an ultrasound system, the microscopic system is essential for the calibration of the ultrasound system. First, our microscopic system is calibrated. The microscopic system includes a Sony XCD-X710 (Sony Corporation, Tokyo, Japan) 1024×768 pixels FireWire camera. This camera is mounted on a Mitutoyo FS70 microscope unit (Mitutoyo, Kawasaki, Japan) using a Mitutoyo M Plan Apo 2× / 0.055 Objective. The water reservoir is replaced with a marker plate to determine the absolute orientation and position of the setup with respect to the camera. This calibration results in an accuracy of 2.34 μm per pixel. Second, our ultrasound system allows for drawing lines with known dimensions. This option allows us to calculate the microns to pixel ratio from the ultrasound images. This procedure results in a ratio of 20.98 μm per pixel for the ultrasound system. Third, We verify the correctness of this simple calibration procedure by simultaneously acquiring the motion of the microparticles using our calibrated microscopic system and the ultrasound system. The calibrated ultrasound system is used to provide feedback to a closed-loop magnetic-based control system. Parameters of the ultrasound system are included in Table I.

III. MOTION CONTROL RESULTS

Motion control of paramagnetic microparticles is implemented through the magnetic-force current map (2). We devise a proportional-derivative control force ($\mathbf{F}(\mathbf{P}) \in \mathbb{R}^{2\times 1}$) of the following form [17]:

$$\mathbf{F}(\mathbf{P}) = \mathbf{K_p} \mathbf{e} + \mathbf{K_d} \dot{\mathbf{e}}, \tag{4}$$

where $\mathbf{K_p} \in \mathbb{R}^{2\times 2}$ and $\mathbf{K_d} \in \mathbb{R}^{2\times 2}$ are the controller positive-definite gain matrices. Further, $\mathbf{e} \in \mathbb{R}^{2\times 1}$ and $\dot{\mathbf{e}} \in$

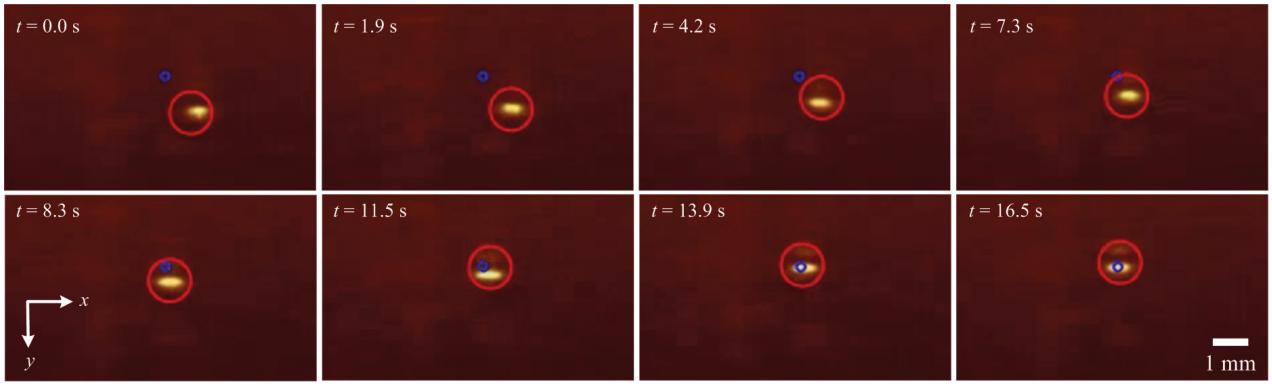

Fig. 4. Magnetic-based closed-loop motion control of a paramagnetic microparticle using ultrasound feedback. The microparticle moves towards the reference position (blue circle) under the influence of the magnetic field gradients generated using control law (4). Diameter of this microparticle is approximately 100 μm. However, the size in the ultrasound image is larger due to artifacts. The microparticle moves at an average speed of 191 μm/s. The microparticle starts its motion at the time instant, $t = 0.0$ seconds, and is positioned within the vicinity of the reference position starting from the time instant, $t = 11.5$ seconds. The maximum position tracking error in the steady state is 199 μm. *Please refer to the accompanying video that demonstrates the point-to-point motion control of a microparticle using ultrasound feedback.*

$\mathbb{R}^{2\times1}$ are the position and velocity tracking errors, respectively. These errors are calculated based on the feedback provided by the ultrasound system. The position tracking error $(\mathbf{e})$ and velocity tracking error $(\dot{\mathbf{e}})$ are given by

$$\mathbf{e} = \mathbf{P}_{\text{us}} - \mathbf{P}_{\text{ref}} \quad \text{and} \quad \dot{\mathbf{e}} = \dot{\mathbf{P}}_{\text{us}}. \tag{5}$$

In (5), $\mathbf{P}_{\text{ref}} \in \mathbb{R}^{2\times1}$ is a fixed reference position. Further, $\mathbf{P}_{\text{us}} \in \mathbb{R}^{2\times1}$ and $\dot{\mathbf{P}}_{\text{us}} \in \mathbb{R}^{2\times1}$ are the position and velocity of the microparticle, respectively. Position of the microparticle is provided using the ultrasound system, whereas the velocity is calculated and supplied to the control system. The control law (4) allows our magnetic system to pull a microparticle towards the reference position using the magnetic field gradients using ultrasound feedback. A representative point-to-point motion control of a microparticle is shown in Fig. 4. Position of the microparticle is determined (red circle is assigned by our feature tracking algorithm) using the ultrasound images and provided to the closed-loop control system. The magnetic system pulls the microparticle towards the reference position (small blue circle) by the magnetic field gradients at an average speed of 191 μm/s. At time instant, $t = 11.5$ seconds, the microparticle reaches the reference position and the control system localizes the microparticle within the vicinity of the reference position.

TABLE I

PARAMETERS OF THE ULTRASOUND SYSTEM (SIEMENS ACUSON S2000, SIEMENS HEALTHCARE, MOUNTAIN VIEW, USA) USING THE 18L6 HD PROBE. ADVANCED SIECLEAR$^{\text{TM}}$: SPATIAL COMPOUNDING TECHNOLOGY UTILIZES MULTIPLE LINES OF SIGHT TO IMPROVE CONTRAST RESOLUTION AND BORDER DETECTION. DYNAMIC TISSUE CONTRAST ENHANCEMENT (TCE)$^{\text{TM}}$: PROVIDES ADVANCED SPECKLE REDUCTION AND COMBINATION WITH ENHANCED CONTRAST RESOLUTION. EDGE: APPLIES EDGE ENHANCEMENT. SPACE/TIME: DEFINES SPATIAL RESOLUTION VERSUS TEMPORAL RESOLUTION. MAPS: SELECTS A PROCESSING CURVE THAT ASSIGNS ECHO AMPLITUDES TO GRAYSCALE LEVELS. TINT: COLORIZES THE GRAY SCALE IMAGE.

Advanced Sieclear$^{\text{TM}}$	Dynamic TCE$^{\text{TM}}$	Edge	Space Time	Maps	Tint	Zoom
13	High	4	3	D	5	Max.

Another representative point-to-point motion control result is shown in Fig. 5(a). Motion of the microparticle is provided to the control system to determine the position tracking error using (5) based on the ultrasound system and the microscopic vision system. The microparticle is controlled at an average speed of 125 μm/s and 191 μm/s using the microscopic and ultrasound feedback, respectively. We observe that the magnetic-based control system achieves maximum position tracking error of 199 μm in the steady-state using ultrasound feedback. For the same controller gains, maximum position tracking error of 79 μm is achieved using microscopic feedback (Fig. 5(b)). We attribute the difference in the positioning accuracy between the ultrasound- and microscopic-guided magnetic-based control to the accuracy of the feature tracking of each imaging systems. We use similar feature tracking algorithm [11] to determine the position of the microparticle from images acquired from the ultrasound and the microscopic systems (Section II-B). *Please refer to the accompanying video that demonstrates the point-to-point motion control of a microparticle using ultrasound feedback.*

In order to demonstrate that the configuration of the electromagnetic coils allows the microparticles to be controlled within the entire workspace, we devise different trajectories as shown in Fig. 6. Motion control using ultrasound and microscopic feedback is done by providing way-points (black circles) to the control system. We observe that the controlled microparticles follows a sinusoidal trajectory at an average speed of 94 μm/s and 90 μm/s using the ultrasound and microscopic feedback, respectively (Fig. 6(a)). Fig. 6(b) shows an ultrasound- and microscopic-guided magnetic-based control of an s-trajectory using 6 way points. The controlled

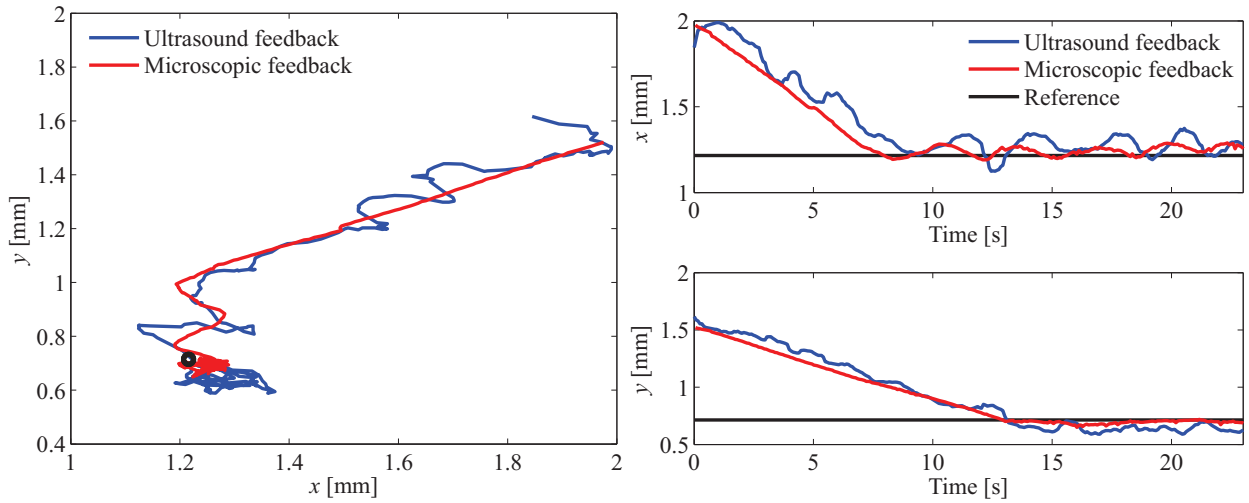

(a) Path of the controlled microparticle

(b) Position of the microparticle along x- and y-axis

Fig. 5. Motion control of a paramagnetic microparticle based on the feedback provided by an ultrasound system and a microscopic system. (a) The average speed of the controlled microparticle using ultrasound and microscopic feedback is 125 μm/s and 191 μm/s, respectively. The small black circle represents the reference position. (b) In the steady-state, the maximum position tracking error is 199 μm and 79 μm using ultrasound and microscopic feedback, respectively. *Please refer to the accompanying video that demonstrates the point-to-point motion control of a microparticle using ultrasound feedback and the tracked motion using the microscopic system.*

microparticle follows this trajectory at an average speed of 115 μm/s and 113 μm/s using the ultrasound and microscopic feedback, respectively. Finally, we demonstrate the motion control of a zig-zag trajectory (Fig. 6(b)) at an average speed of 279 μm/s and 206 μm/s using the ultrasound and microscopic feedback, respectively. The deviation between the average speeds calculated based on the ultrasound- and microscopic-based control systems is due to the undesirable motion artifacts that are often observed in the ultrasound images. The averages are calculated from 5 closed-loop motion control trials for each feedback system. Table II includes the results of the closed-loop motion control of microparticles. *Please refer to the accompanying video that demonstrates the control of a microparticle using ultrasound feedback and the tracked motion using the microscopic system.*

Positioning accuracy of the microscopic-based control system is approximately 52% better than that of the ultrasound-based control system. We attribute this difference to 2 aspects, i.e., the microns to pixel ratio and the undesirable motion artifacts. Calibration of the microscopic and ultrasound system shows that the former provides 2.34 μm per pixel, whereas the later provides 20.98 μm per pixel. Unlike the feedback provided by the microscopic system, the ultrasound feedback is distorted by the artifacts that limits the accuracy of our closed-loop motion control system. A microparticle with a diameter of 53 μm appears as a bright spot with a diameter of 608 μm using the ultrasound parameters provided in Table I. These parameters are adjusted online to distinguish between microparticles and the undesirable artifacts, and to increase the brightness of the microparticles within the workspace. Due to these inevitable artifacts, accuracy of the ultrasound-based control is evaluated by a microscopic system. The motion control is implemented based on the feedback provided by the ultrasound system, and motion of the controlled microparticles is also determined using the microscopic system to validate the accuracy of the ultrasound-based closed-loop control system.

TABLE II

AVERAGE VELOCITIES AND MAXIMUM POSITION TRACKING ERRORS OF THE CONTROLLED MICROPARTICLES USING MICROSCOPIC AND ULTRASOUND FEEDBACK. VELOCITIES ARE CALCULATED FOR AN S-TRAJECTORY, A ZIG-ZAG TRAJECTORY, AND A SINUSOIDAL TRAJECTORY.

Trajectory	Feedback	Axis	Average velocity (μm/s)	Error (μm)
Sinusoidal	Microscope	x	84.6 ± 40.2	29.1
		y	31.3 ± 22.6	63.4
		Absolute	90.2 ± 41.5	71.6
	Ultrasound	x	87.6 ± 65.1	25.8
		y	34.7 ± 32.6	57.6
		Absolute	94.4 ± 66.1	64.7
S	Microscope	x	108.1 ± 55.4	10.2
		y	33.8 ± 33.1	38.3
		Absolute	113.3 ± 51.7	25.9
	Ultrasound	x	104.8 ± 81.4	11.1
		y	46.4 ± 40.2	30.7
		Absolute	114.6 ± 77.8	22.0
Zig-zag	Microscope	x	185.2 ± 63.0	23.6
		y	89.9 ± 44.4	55.0
		Absolute	205.8 ± 67.4	59.8
	Ultrasound	x	235.0 ± 201.1	10.1
		y	150.9 ± 136.9	23.5
		Absolute	279.3 ± 220.5	25.6

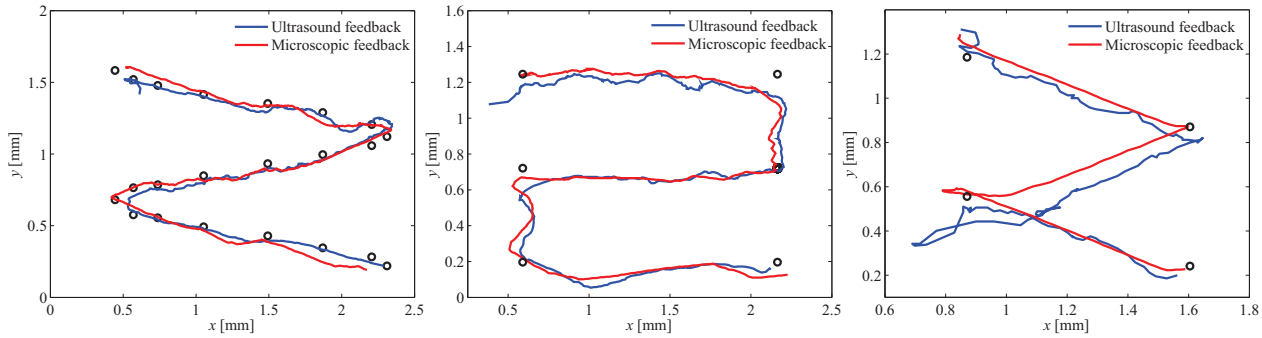

(a) Sinusoidal trajectory (b) S-trajectory (c) Zig-zag trajectory

Fig. 6. Motion control of a paramagnetic microparticle based on the feedback provided by an ultrasound system and a microscopic system. Way points (black circles) are provided to the control system to define the trajectory. (a) Controlled microparticle following a sinusoidal trajectory at average speeds of 94 μm/s and 90 μm/s for the ultrasound- and microscopic-based control, respectively. (b) Controlled microparticle following an s-trajectory at average speeds of 115 μm/s and 113 μm/s for the ultrasound- and microscopic-based control, respectively. (c) Controlled microparticle following a zig-zag trajectory at average speeds of 279 μm/s and 206 μm/s for the ultrasound- and microscopic-based control, respectively. *Please refer to the accompanying video that demonstrates the point-to-point motion control of a microparticle using ultrasound feedback and the tracked motion using the microscopic system.*

IV. CONCLUSIONS AND FUTURE WORK

Wireless magnetic-based motion control of paramagnetic microparticles is achieved using ultrasound feedback. A magnetic system is adapted to provide feedback from an ultrasound system and a microscopic system. This adaptation allows us to achieve point-to-point motion control of microparticles based on the feedback provided by the ultrasound system. Furthermore, it allows us to evaluate the accuracy of the ultrasound-based control system using the microscopic-based controller. Despite the inevitable motion artifacts we obtain in the ultrasound feedback, the motion control system achieves point-to-point motion control at an average speed and average position tracking error of 191 μm/s and 48 μm using ultrasound feedback, respectively.

As part of future work, a three-dimensional (3D) magnetic system will be modified to provide feedback from an ultrasound system. This modification will allow us to control paramagnetic microparticles and microrobots in 3D space using ultrasound feedback. Furthermore, motion control of microparticles and nanoparticles will be achieved in fluidic microchannels with time-varying flow rates [6], [8] based on the feedback provided by the ultrasound system.

REFERENCES

[1] S. Martel, O. Felfoul, J.-B. Mathieu, A. Chanu, S. Tamaz, M. Mohammadi, M. Mankiewicz, and N. Tabatabaei, "MRI-based medical nanorobotic platform for the control of magnetic nanoparticles and flagellated bacteria for target interventions in human capillaries," *International Journal of Robotics Research*, vol. 28, no. 9, pp. 1169-1182, September 2009.

[2] J.-B. Mathieu and S. Martel, "Steering of aggregating magnetic microparticles using propulsion gradients coils in an MRI scanner," *Magnetic Resonance in Medicine*, vol. 63, no. 5, pp. 1336-1345, May 2010.

[3] B. J. Nelson, I. K. Kaliakatsos, and J. J. Abbott, "Microrobots for minimally invasive medicine," *Annual Review of Biomedical Engineering*, vol. 12, pp. 55-85, April 2010.

[4] M. P. Kummer, J. J. Abbott, B. E. Kartochvil, R. Borer, A. Sengul, and B. J. Nelson, "OctoMag: an electromagnetic system for 5-DOF wireless micromanipulation," *IEEE Transactions on Robotics*, vol. 26, no. 6, pp. 1006-1017, December 2010.

[5] J. Wang and W. Gao, "Nano/microscale motors: biomedical opportunities and challenges," *ACS Nano*, vol. 6, no. 7, pp. 5745-5751, July 2012.

[6] S. Sanchez, A. A. Solovev, S. M. Harazim, and O. G. Schmidt, "Microrobots swimming in the flowing streams of microfluidic channels," *Journal of the American Chemical Society*, vol. 133, no. 4, pp. 701-703, December 2010.

[7] I. S. M. Khalil, V. Magdanz, S. Sanchez, O. G. Schmidt, and S. Misra, "Control of self-propelled microjets inside a microchannel with time-varying flow rates," *IEEE Transactions on Robotics*. DOI:10.1109/TRO.2013.2281557. *In Press*

[8] I. S. M. Khalil, M. P. Pichel, O. S. Sukas, L. Abelmann, and S. Misra, "Control of magnetotactic bacterium in a micro-fabricated maze," in *Proceedings of the IEEE International Conference on Robotics and Automation (ICRA)*, pp. 5488-5493, Karlsruhe, Germany, May 2013.

[9] M. Evertsson, M. Cinthio, S. Fredriksson, F. Olsson, H. W. Persson, and T. Jansson, "Frequency- and phase-sensitive magnetomotive ultrasound imaging of superparamagnetic iron oxide nanoparticles," in *IEEE Transactions on Ultrasonics, Ferroelectrics, and Frequency Control*, vol. 60, no. 3, pp. 481–491, March 2013.

[10] J. Weizenecker, B. Gleich, J. Rahmer, H. Dahnke, and J. Borgert, "Three-dimensional real-time in *vivo* magnetic particle imaging," *Physics in Medicine and Biology*, vol. 54, no. 5, pp. 1–10, March 2009.

[11] J. D. Keuning, J. de Vries, L. Abelmann, and S. Misra, "Image-based magnetic control of paramagnetic microparticles in water," in *Proceedings of the IEEE/RSJ International Conference of Robotics and Systems (IROS)*, pp. 421-426, San Francisco, USA, September 2011.

[12] I. S. M. Khalil, J. D. Keuning, L. Abelmann, and S. Misra, "Wireless magnetic-based control of paramagnetic microparticles," in *Proceedings of the IEEE RAS/EMBS International Conference on Biomedical Robotics and Biomechatronics (BioRob)*, pp. 460-466, Rome, Italy, June 2012.

[13] I. S. M. Khalil, R. M. P. Metz, L. Abelmann, and S. Misra, "Interaction force estimation during manipulation of microparticles," in *Proceedings of the IEEE International Conference of Robotics and Systems (IROS)*, pp. 950-956, Vilamoura, Portugal, October 2012.

[14] D. Jiles, "Introduction to magnetism and magnetic materials", Taylor & Francis, 1998.

[15] T. H. Boyer, "The force on a magnetic dipole," *American Journal of Physics*, vol. 56, no. 8, pp. 688-692, August 1988.

[16] S. S. Shevkoplyas, A. C. Siegel, R. M. Westervelt, M. G. Prentiss, and G. M. Whitesides, "The force acting on a superparamagnetic bead due to an applied magnetic field," *Lab on a Chip*, vol. 7, no. 6, pp. 1294-1302, July 2007.

[17] I. S. M. Khalil, V. Magdanz, S. Sanchez, O. G. Schmidt, L. Abelmann and S. Misra, "Magnetic control of potential microrobotic drug delivery systems: nanoparticles, magnetotactic bacteria and self-propelled microjets," in *Proceedings of the International Conference of the IEEE Engineering in Medicine and Biology Society (EMBC)*, pp. 5299-5302, Osaka, Japan, July 2013.